Research

New Phytologist

Long-lasting impact of chitooligosaccharide application on strigolactone biosynthesis and fungal accommodation promotes arbuscular mycorrhiza in *Medicago truncatula*

Veronica Volpe[1], Matteo Chialva[1], Teresa Mazzarella[1], Andrea Crosino[1], Serena Capitanio[1], Lorenzo Costamagna[1], Wouter Kohlen[2] and Andrea Genre[1]

[1]Department of Life Sciences and Systems Biology, University of Turin, Viale Mattioli 25, 10125 Torino, Italy; [2]Laboratory of Molecular Biology, Wageningen University & Research, Wageningen 6708, PB, the Netherlands

Author for correspondence:
Andrea Genre
Email: andrea.genre@unito.it

Received: *25 October 2022*
Accepted: *13 December 2022*

New Phytologist (2023) **237:** 2316–2331
doi: 10.1111/nph.18697

Key words: arbuscular mycorrhiza, chitooligosaccharides, *Medicago truncatula*, strigolactones, symbiosis.

Summary

- The establishment of arbuscular mycorrhiza (AM) between plants and Glomeromycotina fungi is preceded by the exchange of chemical signals: fungal released Myc-factors, including chitooligosaccharides (CO) and lipo-chitooligosaccharides (LCO), activate plant symbiotic responses, while root-exuded strigolactones stimulate hyphal branching and boost CO release. Furthermore, fungal signaling reinforcement through CO application was shown to promote AM development in *Medicago truncatula*, but the cellular and molecular bases of this effect remained unclear.
- Here, we focused on long-term *M. truncatula* responses to CO treatment, demonstrating its impact on the transcriptome of both mycorrhizal and nonmycorrhizal roots over several weeks and providing an insight into the mechanistic bases of the CO-dependent promotion of AM colonization.
- CO treatment caused the long-lasting regulation of strigolactone biosynthesis and fungal accommodation-related genes. This was mirrored by an increase in root didehydro-orobanchol content, and the promotion of accommodation responses to AM fungi in root epidermal cells. Lastly, an advanced downregulation of AM symbiosis marker genes was observed at the latest time point in CO-treated plants, in line with an increased number of senescent arbuscules.
- Overall, CO treatment triggered molecular, metabolic, and cellular responses underpinning a protracted acceleration of AM development.

Introduction

Mineral nutrition of most plants is supported by the mutualistic root symbiosis with Glomeromycotina, an ancient group of soil fungi (Spatafora *et al.*, 2016) that grant their host plants preferential access to soil inorganic nutrients, in change for plant-photosynthesized sugars and lipids (Smith & Read, 2008; Wewer *et al.*, 2014; Keymer *et al.*, 2017).

Plant–fungus recognition is essential for arbuscular mycorrhiza (AM) establishment and is based on an exchange of chemical signals (Bonfante & Requena, 2011; Zipfel & Oldroyd, 2017). On the one hand, root-exuded strigolactones (SL), a class of terpenoid lactones, signal host proximity (Akiyama *et al.*, 2005) activating hyphal metabolism and branching, and eventually promoting physical encounter with the root surface (Besserer *et al.*, 2006; Waters *et al.*, 2017). On the other hand, AM fungi release diffusible molecules (Myc-factors) that activate a so-called Common Symbiotic Signalling Pathway, or CSSP (Zipfel & Oldroyd, 2017; Choi *et al.*, 2018). Downstream responses include local and systemic changes in gene expression and metabolism, overall preparing the host plant to symbiosis establishment (MacLean *et al.*, 2017; Choi *et al.*, 2018; Pimprikar & Gutjahr, 2018).

Myc-factors include two classes of molecules: lipo-chitooligosaccharides, or LCO (Maillet *et al.*, 2011), structurally similar to rhizobial Nod-factors and composed of a short chitin chain with a few lateral substitutions, and short-chain chitooligosaccharides, or CO (Genre *et al.*, 2013), where only the chitin backbone is present. The activity of CO as AM fungal signals has been demonstrated in all tested host plants, including monocots and dicots (Sun *et al.*, 2015; Nasir *et al.*, 2021) and their release is boosted upon strigolactone perception (Genre *et al.*, 2013). Furthermore, CO can easily be produced through chitin hydrolysis (Crosino *et al.*, 2021) making them particularly interesting for large-scale agricultural applications (Volpe *et al.*, 2020). Indeed, our recent research project AM for Quality explored the effects of exogenous CO application on AM development in forage plants by running field treatments (V. Volpe & A. Genre, unpublished) alongside laboratory experiments, all based on a CO mix with the same

composition and concentration. CO treatment before fungal inoculation promoted a marked increase in arbuscule development, biomass accumulation, and total photosynthetic surface, than untreated mycorrhizal plants, in both field and laboratory conditions over several weeks (Volpe *et al.*, 2020). At present, most researches have investigated plant responses to CO or LCO treatment on a shorter time scale, demonstrating the activation of symbiotic signaling and gene regulation in the range of a few hours (Czaja *et al.*, 2012; Camps *et al.*, 2015; Giovannetti *et al.*, 2015; Feng *et al.*, 2019).

Here, we chose to focus on a longer time scale, in an attempt to track the molecular bases of the observed CO-dependent promotion of AM development over several weeks (Volpe *et al.*, 2020). To this aim, we used RNA-seq to investigate genome-wide changes in root gene expression over four weeks after the initial short-chain CO treatment, and further validated our results with functional insights. CO treatment changed the expression pattern of the whole strigolactone biosynthetic pathway and increased the didehydro-orobanchol content in root tissue. Moreover, RNA-seq data, targeted gene expression analyses, and live imaging of epidermal cell reorganization indicated a CO-dependent stimulation of intracellular accommodation processes. Lastly, the downregulation of AM symbiosis marker genes was consistent with the increased number of senescent arbuscules at the end of our experimental time frame. In conclusion, our results revealed that CO treatment impacted on molecular, cellular, and metabolic mechanisms that converged toward a global acceleration in AM development.

Materials and Methods

Plant and fungal materials

The model legume *Medicago truncatula* cv 'Jemalong' (line A17) was used for this study. Seeds were collected from the pods, kept for 2 d at room temperature to allow the oxygenation of internal tissues and scarified on sandpaper in order to break the seed coat. Seeds were then sterilized using 5% (v/v) sodium hypochlorite in sterile water and rinsed in sterile distilled water, each step for 5 min keeping the falcon tubes under constant stirring. To break dormancy and allow rapid and synchronized germination, seeds were placed on 0.6% Plant-Agar (Duchefa, Haarlem, the Netherlands) plates, maintained at 4°C in the dark for 2 d and then moved at 23°C until germination.

A commercial granular inoculum of the AM fungus *Funneliformis mosseae* (strain BEG 12) from MycAgroLab (www.mycagrolab.com; France) was used for all experiments. The inoculum consisted of growth substrate of *Sorghum vulgare* plants, colonized root pieces, spores, and extraradical mycelium, with a minimum of 10 active propagules per g of inoculum.

Chitin oligomers

A mixture of short-chain chitooligosaccharides, CO (Volpe *et al.*, 2020), was used for all plant treatments. The CO mixture was obtained from crustacean food manufacturing waste (Zhengzhou Sigma Chemical Co. Ltd, Zhengzhou, Henan, China) and contained fully acetylated, mono-deacetylated, and di-deacetylated molecules composed of 2–5 *N*-acetyl-glucosamine residues (Volpe *et al.*, 2020). Chitooligosaccharides were applied as a 1 g l^{-1} solution in sterile distilled water supplemented with Tween 20 (0.005%) as a surfactant. Sterile water with Tween 20 (0.005%) was used in control treatments.

Pot culture

Young *M. truncatula* seedlings were transferred into 9 cm × 9 cm × 12 cm pots (one seedling per pot) filled with sterile coarse sand (0.4–0.8 mm; Valle Po, Revello, CN, Italy). A plastic bag was placed on the pots during the first week, to protect the young plants from desiccation. Plants were grown in phytochambers under controlled conditions (23°C : 21°C, day : night temperature, 16 h : 8 h, light : dark photoperiod) and fertilized once per week using a modified Long Ashton (LA) nutrient solution (Hewitt, 1966) containing 3.2 μM phosphate and 1 mM nitrate. During the rest of the week, pots were watered when necessary with tap water.

Four experimental conditions were set up: control (CTR) plants, lacking both CO treatment and AM inoculation; CO-treated control (CTR + CO); mycorrhizal (MYC), where AM inoculum was added in the absence of CO treatments; and CO-treated mycorrhizal (MYC + CO), where plants were both inoculated and exposed to the CO solution. Chitooligosaccharides treatment and fungal inoculum were applied as previously described by Volpe *et al.* (2020). In short, 5 ml of CO solution were sprayed over the pot substrate surface 4 and 2 d before inoculation with 22.5 ml of fungal inoculum.

Plants were harvested at 10, 14, 21, 28 d postinoculation (dpi) and carefully washed under tap water to remove sand. Arbuscular mycorrhiza colonization was assessed based on the presence of root-bound extraradical mycelium before rapid sampling, dip-freezing in liquid nitrogen, and storage at −80°C until RNA extraction. We used five plants for each experimental condition at each time point, except at 10 dpi, when the limited extension of root systems required the sampling of a larger number of plants (12). We collected at least three biological replicates (plants) for each condition, selecting the best developed plants, with no visible sign of pathogenesis or stress and an extensive extraradical fungal development.

RNA isolation and sequencing

Total RNA was extracted from all samples using the RNeasy™ Plant Mini kit (Qiagen). Samples were mechanically homogenized using a TissueLyser system for 2 min at 18 Hz. An aliquot of each sample was mixed with RLT buffer (Qiagen), and further treated following the manufacturer's protocol. RNA quantity and quality were spectrophotometrically checked using a NanoDrop ND-1000 instrument (ThermoFisher Scientific, Rodano, Italy). RNA samples were further quantified and tested for integrity by capillary electrophoresis using Agilent 2100 Bioanalyzer instrument with the Agilent RNA 6000 Nano Kit (Agilent Technologies Italia Spa, Cernusco sul Naviglio, Italy) following the manufacturer's instructions. As requested by the sequencing company (IGATech, Udine, Italy), samples dedicated to RNA-seq were not treated with DNase.

RNA-seq analysis on root RNA samples was performed at IGA Technology services. TruSeq stranded mRNA kit (Illumina, San Diego, CA, USA) was used for library preparation and sequencing performed using Illumina NextSeq 500 platform (Illumina) in single-end mode at 75 bp read-length and with a sequencing depth ranging from 20 to 30 M of reads per sample (Supporting Information Table S1).

Bioinformatics

Adapter sequences were masked with CUTADAPT v.1.11 (Martin, 2011) from raw reads using the following parameters: –anywhere (on both adapter sequences) –overlap 5-times 2 –minimum-length 35-mask-adapter. Raw reads were then trimmed removing lower quality bases and adapters using the ERNE software (Del Fabbro *et al.*, 2013). The expression level of each gene in each library was calculated by mapping filtered reads on Mt4.1 reference genome (Young *et al.*, 2011; Tang *et al.*, 2014) using STAR splice-aware aligner (Dobin *et al.*, 2013) with default parameters. Reads overlapping with annotated exons were counted using HTSEQ (Anders *et al.*, 2015) and differential expression analysis performed for each comparison (CTR + CO vs CTR, MYC vs CTR, MYC + CO vs CTR and MYC + CO vs MYC) at each time points (10, 14, 21, 28 dpi) using the DESEQ2 R package (Love *et al.*, 2014) at a False discovery rate (FDR or adjusted *P*-value) (Benjamini & Hochberg, 1995) threshold of 0.05 (Datasets S1–S4). The RNA-seq dataset obtained in this study was included in the Medicago Expression Atlas (MtExpress V3; Carrere *et al.*, 2021).

Differentially expressed genes were plotted into KEGG (Kyoto Encyclopedia of Genes and Genomes) pathway maps using the PATHVIEW R package (Luo & Brouwer, 2013) and the *M. truncatula* annotation available at the KEGG website. Metabolic pathways visualization was achieved using MAPMAN software (Usadel *et al.*, 2005). MAPMAN functional annotation for *M. truncatula* (Table S2) was obtained from the proteome using MERCATOR4 annotation tool (Schwacke *et al.*, 2019).

Gene ontology (GO) enrichment analyses were carried out on each of the previously generated contrasts using the GOSEQ R package (Young *et al.*, 2010) at a FDR cutoff of 0.1. The $-\log_{10}$ of the corrected *P*-value was plotted.

Variance partitioning analysis (VPA) was performed using the 'varpart' function in the R package VEGAN (Oksanen *et al.*, 2019) using gene counts normalized with DESEQ2 through the Variance Stabilizing Transformation (vst). Fractions of variance explained by single factors were tested for significance on the RDA model using permutational ANOVA (999 permutation, $P < 0.05$). Principal component analysis (PCA) was calculated with the 'prcomp' function in the BASE R package, using same normalization used for VPA. Statistical and graphical elaborations were performed in R programming environment (R Core Team, 2020) using the GGPLOT2 package (Wickham, 2016).

Gene expression analysis by real-time qPCR

RNA-seq data were validated by quantitative real-time PCR (qRT-PCR) analysis of the expression profile of 10 differentially expressed genes (DEGs) across all treatments and time points (Fig. S1).

Specific primers (listed in Table S3) were designed using PERLPRIMER software (http://perlprimer.sourceforge.net) on *M. truncatula* CDS sequences from NCBI (http://www.ncbi.nlm.nih.gov/) and *M. truncatula* genome database (http://www.medicagogenome.org). All primers were first tested by PCR on genomic *M. truncatula* and *F. mosseae* DNA, to confirm their plant-specificity.

To remove any trace of genomic DNA before cDNA synthesis, RNA samples were treated with Turbo™ DNase (Qiagen) according to the manufacturer's instructions, followed by second NanoDrop quantification. The RNA samples were routinely checked for DNA contamination by PCR analysis, using primers *MtTEF-F*: 5′-AAGCTAGGAGGTATTGAAAG-3′ and *MtTEF-R*: 5′-ACTGTGCAGTAGTACTTGGTG-3′ for *MtTEF* (Elongation Factor, NCBI Ref. Seq.: XM_013595882).

For single-strand cDNA synthesis, *c.* 700 ng of total RNA was denatured at 65°C for 5 min and then reverse-transcribed using the Super-Script II kit (Invitrogen) at 25°C for 10 min, 42°C for 50 min, and 70°C for 15 min. The final volume was 20 µl volume and contained 10 µM of random primers, 0.5 mM deoxynucloside triphosphates, 4 µl 5× buffer, 2 µl 0.1 M dithiothreitol (DTT), and 1 µl Superscript II enzyme Control PCR was set with TEF primers to test the presence of cDNA.

To confirm the results of our transcriptomic analysis of SL biosynthesis and transport-related genes, root systems from CTR and CTR + CO plants were sampled at 21 dpi in an independent experiment. Hundred milligrams of root powder was used for RNA extraction and analyzed by qRT-PCR.

Lastly, in order to monitor local, short-time occurrence of early gene regulation in response to CO perception, 1 g l^{-1}, 1 mg l^{-1} or 1 µg l^{-1} CO solutions were applied to WT and *dmi3-1 Agrobacterium rhizogenes*-transformed root organ cultures (ROCs) expressing the nuclear targeted NUPYC2.1 protein (Sieberer *et al.*, 2009), which was used as a visual reporter of cell viability. Root organ culture lines were propagated on M medium (Bécard & Fortin, 1988) at 25°C in the dark, in vertically oriented petri dishes to favor the regular fishbone-shaped root system (Chabaud *et al.*, 2002) and grown for 3 wk. For local CO treatment, small disks of filter paper (Ø 4 mm) soaked in 20 µl of CO solution were applied on several lateral roots, 10–15 mm from the root tip, following Chabaud *et al.* (2011). Six hours later, 1-cm-long root segments underlying each disk were excised, immediately frozen, and stored at −80°C until RNA extraction and analysis for the expression of AM fungal perception and accommodation marker genes.

qRT-PCR analyses were performed according to the Rotor-Gene SYBR Green PCR Kit instructions (Qiagen) and were run in a final volume of 15 µl for each tube containing 7.5 µl of Rotor-Gene SYBR Green PCR Master Mix, 5.5 µl of 3 µM specific primers mix (Table S4), and 10 ng of cDNA. A Rotor Gene machine (Qiagen) was used with the following program: 3-min preincubation at 95°C, followed by 40 cycles of 15 s at 95°C, and 30 s at 60°C. Each amplification was followed by melting curve analysis (60–94°C) with a heating rate of 0.5°C every 15 s. All reactions were performed with two technical replicates, and only C_t values with a standard deviation that did not

exceed 0.5 were considered. Relative RNA levels were calibrated using the elongation factor (TEF) mRNA as endogenous reference and normalized to the control line. Results were validated statistically using the unpaired Student's *t*-test to compare two means: differences were considered significant at $P < 0.05$.

Strigolactone analysis in root systems and exudates

CTR and CTR + CO plants were twice, respectively, treated with water or CO solution, and then grown for 21 d. Twenty-one-day-old *M. truncatula* plants were carefully sampled and washed free of sand. They were put inside a tube (two plants for tube) with 40 ml of LA solution covering the whole root system and closed with Parafilm; the tubes were placed into a closed Magenta box and the root system was covered with a black shield. Plants (four biological replicates for each treatment) were placed in a growth chamber for 36 h for exudate collection. After 36 h, the root exudate was recovered and stored at −20°C for the next step.

Whole plant fresh weight (FW), as well as shoot and root biomass separately, was measured for each biological replicate, before each root system was ground to a fine powder in a mortar using liquid nitrogen and stored at −80°C.

For the analysis of SL content, 500 mg of each ground sample was transferred to 2-ml Eppendorf tubes, and SL were extracted with 2 ml of ethyl acetate with 10^{-8} M GR24 as internal standard (end concentration 10^{-7} M). Tubes were vortexed, sonicated for 20 s (Branson Ultrasonics sonication bath; Emerson Automation Solutions, Busseno, Italy), and centrifuged for 10 min at 2500 ***g*** at RT. Subsequently, the organic phases were transferred to 4-ml glass vials, and the solvent was evaporated in a speed vacuum system (SPD121P; ThermoSavant, Hastings, UK). Root exudates were purified and concentrated as previously described for tomato (Kohlen *et al.*, 2012); SL from root tissues and exudates were quantified according to Liu *et al.* (2011).

Live imaging of prepenetration responses

To further investigate whether CO treatment altered cell responses to fungal contact, we modified the targeted AM inoculation technique used by Genre *et al.* (2005, 2008) for visualizing the prepenetration apparatus (PPA) in WT roots. In short, *Agrobacterium rhizogenes*-transformed ROCs expressing the endoplasmic reticulum-targeted GFP-HDEL (Haseloff *et al.*, 1997) were grown on M medium (Boisson-Dernier *et al.*, 2001) in vertically oriented Petri dishes and inoculated with pregerminated spores of *Gigaspora margarita*. One milliliter of filtered CO solution (1 mg l^{-1}) or sterilized water (as control) was then added over the root culture before covering it with a gas-permeable plastic film (bioFOLIE 25; Sartorius, Goettingen, Germany). Fungus–root interaction was monitored daily using a stereomicroscope and contact sites were imaged at 7, 10, and 14 dpi using a Leica TCS SP2 confocal microscope fitted with a long distance ×40 water-immersion objective (HCX Apo 0.80). GFP fluorescence was excited with the argon laser band at 488 nm and recorded with an emission window set at 500–525 nm.

Morphological and functional analysis of AM colonization

Total and root fresh biomass were measured in mycorrhizal WT plants in the presence or absence of CO treatment. Biomass data were compared, and the results were validated statistically using the unpaired Student's *t*-test (differences were considered significant at $P < 0.05$). Furthermore, inoculated WT and *dmi3-1* mutant plants, treated or not with CO, were sampled at 28 dpi to quantify fungal colonization according to Trouvelot *et al.* (1986). At least four plants were used for the root mycorrhization intensity assessment and 100 1-cm-long root pieces were analyzed per plant. The same method was adapted for the *dmi3-1* mutant (where intraradical colonization is blocked) to determine frequency (*F*) and intensity (*M*) parameters with reference to hyphopodium presence on the root surface instead of intraradical fungal structures.

For detailed microscope analysis of arbuscule morphology, root segments of WT plants were excised and individually embedded in agarose (5%). Hundred micrometers vibratome sections was then moved to microscope slides and treated for 5 min in phosphate buffer containing 0.5% commercial bleach, rinsed three times, and then incubated overnight in 10 μg ml^{-1} wheat germ agglutinin–fluorescein isothiocyanate (WGA–FITC; Sigma-Aldrich) to label the fungal wall. A Leica TCS SP2 confocal microscope (Leica Microsystems GmbH, Wetzlar, Germany) equipped with a ×40 water immersion objective was used for imaging with fluorescence excitation at 488 nm and acquisition at 500–550 nm.

Results

CO treatment impacted on the root transcriptome for several weeks

In a first global analysis of the RNA-seq dataset, PCA (Fig. 1a) and variance partitioning analysis (VPA; Fig. 1b) revealed a high level of variation in the transcriptome between conditions and time points. As shown in Fig. 1(a), CTR, CTR + CO, MYC, and MYC + CO transcriptomes clustered in different areas of the PCA plot, indicating that both AM inoculation and CO treatment had a strong influence on the root gene expression profiles. In order to grant a homogeneous code for sample timing, we refer to dpi for both inoculated and noninoculated (but same age) plants. At 10 dpi, CTR + CO, MYC, and MYC + CO samples were clearly separated from CTR along the PC1 axis (explaining 33.38% of variance), highlighting the distance in the transcriptional profile of CTR samples compared with the remaining treatments. A major distinction along the PC1 axis became evident since 14 dpi between inoculated (MYC and MYC + CO) and noninoculated samples (CTR and CTR + CO), as expected in relation with AM establishment. A specific effect of the CO treatment was evident at 10 dpi (with a clear separation between CTR and CTR + CO, and a milder but evident separation between MYC and MYC + CO), and partially rebounded at 28 dpi between MYC and MYC + CO samples.

Variance partitioning analysis (Fig. 1b) highlighted time as the most influential variable in our time-course study, in line with

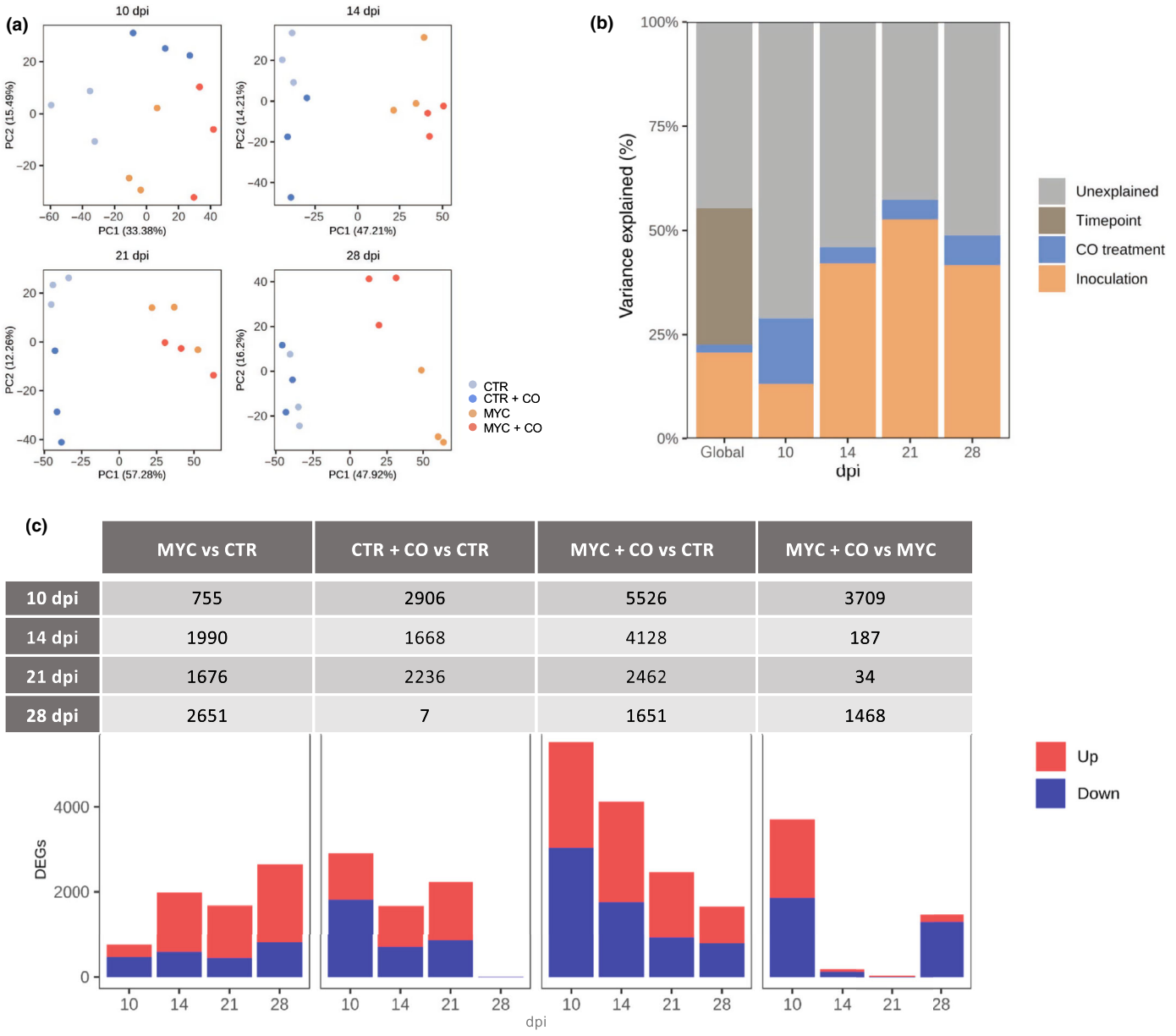

(c)

	MYC vs CTR	CTR + CO vs CTR	MYC + CO vs CTR	MYC + CO vs MYC
10 dpi	755	2906	5526	3709
14 dpi	1990	1668	4128	187
21 dpi	1676	2236	2462	34
28 dpi	2651	7	1651	1468

Fig. 1 Global overview of transcriptomic data. (a) Principal component analysis (PCA) plots highlighted a clear separation of the expression profiles between arbuscular mycorrhiza (AM) inoculated (dark and light orange) and noninoculated (dark and light blue) samples, as well as between treated (dark orange and dark blue) and nontreated (light orange and light blue) ones. Three biological replicates (individual dots) are plotted per condition and time point. (b) Variance partitioning analysis (VPA) considered three factors: AM fungus presence (inoculation), chitooligosaccharides (CO) treatment and time (10, 14, 21, 28 d postinoculation (dpi)). The strongest influence on gene regulation resulted to depend on time, while CO treatment had a major effect at the earliest time point (10 dpi). All the fractions explained by the factors were significant (ANOVA on RDA model, $P < 0.05$), except for the fraction explained by CO treatment at 14 dpi. (c) Differentially expressed genes (DEGs) in the four comparisons and at different time points. Number and expression trend of DEGs. Upregulation is shown in red, downregulation in blue (FDR < 0.05).

the expected major changes in gene expression throughout AM development (Handa *et al.*, 2015). Variance partitioning analysis was subsequently used to address individual time points: this correlated CO treatment to the highest amount of variance in gene regulation at 10 dpi, an early time point in root colonization in our experimental conditions, while AM inoculation became the most influential variable in the later time points. Also in this case, the CO effect extended across all four time points, with a partial reinforcement at 28 dpi.

In conclusion, both PCA and VPA indicated an impact of CO treatment across our whole time-course analysis, with the strongest effect at the earliest time point in both inoculated and noninoculated plants.

The number and proportion of differentially expressed genes (DEGs) among the four conditions at each of the four time points is summarized in Fig. 1(c). The MYC vs CTR comparison highlighted a progressive increase in gene regulation, in line with the ongoing colonization of the root system by the AM fungus.

In the CTR + CO vs CTR comparison, the CO effect was strongest at 10 dpi (with 2906 DEGs), intermediate at 14 and 21 dpi, and minimal at 28 dpi (with only 7 DEGs). This pattern can be explained with the progressive degradation/leaching of CO from the pot over the weeks that follow the initial treatments (4 and 2 d before inoculation). The strongest differences in gene regulation were observed when comparing MYC + CO vs CTR samples (which represent the most dissimilar conditions in our experiment). Here, the strongest impact of the CO treatment was recorded at 10 dpi (5526 DEGs), with a progressive decrease thereafter. This is suggestive of a synergistic effect of exogenous CO and fungal-secreted Myc-factors during early root colonization, and is in line with the progressive decrease of CO effect over time (as highlighted in CTR + CO vs CTR). Lastly, the MYC + CO vs MYC comparison aimed to dissect the effect of exogenous CO on the AM interaction. Also in this case, a major impact was evident at 10 dpi (3709 DEGs), in line with the reinforcement of fungal signaling by the applied CO. Nevertheless, differential gene regulation peaked again at 28 d (1468 DEGs) with a large majority of downregulated sequences, whereas intermediate time points displayed a very similar gene regulation scenario in the two conditions.

In summary, differential gene expression analysis convincingly supported the evidence emerging from multivariate analysis, indicating an impact of CO on plant gene regulation throughout our experimental time frame, with a major effect during early root colonization.

Functional enrichment analysis suggests that CO treatment mimics fungal presence

To gain insights into the molecular processes impacted by CO treatment, we performed a GO enrichment analysis of DEGs (Datasets S5–S8; http://geneontology.org/docs/ontology-documentation/). We will focus here on the two most strongly regulated time points: 10 and 28 dpi, and the most over-represented GO terms for each comparison, as presented in Figs S2–S5. Interestingly, in the MYC vs CTR comparison (Fig. S2), *Defense responses* were over-represented both at 10 and 28 dpi, in agreement with the well-documented regulation of defense-related genes during AM interaction (Salzer *et al.*, 2000; Jung *et al.*, 2012; Cameron *et al.*, 2013). *Protein serine/threonine kinase activity* emerged at 10 and 28 dpi and *DNA-binding transcription factor activity* at 28 dpi, reflecting the extensive impact of symbiosis on regulatory pathways (Liu *et al.*, 2003; Küster *et al.*, 2004; Sanchez *et al.*, 2004; Hohnjec *et al.*, 2005; Hogekamp & Küster, 2013). The whole ubiquitination system (*ubiquitin ligase complex*, *protein ubiquitination*, *ubiquitin protein transferase activity*) was regulated at 28 dpi, possibly indicating the onset of senescence-related mechanisms. Lastly, *fatty acid biosynthesis* appeared at 28 dpi, likely related to both the extensive synthesis of perifungal membranes and the intense production of lipids feeding the fungus (Wewer *et al.*, 2014; Luginbuehl *et al.*, 2017; MacLean *et al.*, 2017).

Since no enriched GO category emerged at 28 dpi for the CTR + CO vs CTR comparison (Fig. S3), we only comment here on the 10 dpi time point. In this case, a remarkable analogy emerged with the same time point of the MYC vs CTR comparison (Fig. S6): in fact, the global pattern of gene regulation was very similar for *kinase activity*, *signal transduction*, *defense response*, and *acyl transferase activity*. This supports the role of CO as mimics of fungal presence and elicitors of symbiotic signaling and gene regulation in the host root.

In the MYC + CO vs CTR comparison at 10 dpi (Fig. S4), a massive activation was observed in protein biosynthesis (*translation*, *ribosome*, *and ribosome constituents*), cytoskeleton-associated processes (*microtubule-associated complex*, *microtubule-based movement*, *and microtubule motor activity*), and chromatin reorganization (*nucleosome*, *and nucleosome assembly*). This is suggestive of intense cell reorganization and is supported by our knowledge of the fungal accommodation process that takes place inside each colonized cell (Gutjahr & Parniske, 2013; Carotenuto *et al.*, 2019). At 28 dpi (Fig. S4), GO terms related to transport (*transporter activity*, *transport*, *heme binding*, *sulfate transport*, *transmembrane transport*, *secondary active sulfate transmembrane transport activity*, and *membrane*) were highly represented, likely related to the extensive AM colonization promoted by CO treatment (Benedito *et al.*, 2010; Gaude *et al.*, 2012; Handa *et al.*, 2015).

Finally, the MYC + CO vs MYC comparison (Fig. S5) suggested that exogenous CO enhanced *cell cycle regulation*, *chromatin rearrangement*, and *cytoskeleton-associated processes* at 10 dpi, hinting at an intensification of the fungal accommodation responses in CO-treated plants. By contrast, a major impact on regulatory and proteolytic processes appeared at 28 dpi in CO-treated plants, suggesting the appearance of senescence-related processes.

In conclusion, our analysis of GO enrichment indicated a global consistency between the regulatory responses induced by AM fungi and CO treatment, with a reinforcement and an advancement of symbiotic processes in plants that were exposed to both stimuli.

CO treatment stimulated strigolactone signaling and fungal accommodation

Among the various gene pathways related to AM establishment that were highlighted by GO enrichment analysis (Table 1), we chose to validate the observed regulation of signaling- and cell reorganization-related genes with functional analyses.

First, we focused on the regulation of Strigolactone (SL) signaling. Strigolactone are carotenoid-derived plant hormones (Gomez-Roldan *et al.*, 2008; Umehara *et al.*, 2008) that also function as extraradical signals to activate AM fungi (Waters *et al.*, 2017). Strigolactone biosynthesis (*CCD8-1* and *CCD8-2*) and transport (*PDR1a*) marker genes were downregulated at 28 dpi in MYC compared with CTR plants (Fig. 2a), which is in line with the inhibition of rhizospheric SL signaling upon maximum root colonization (López-Ráez *et al.*, 2011). Remarkably, this downregulation of SL biosynthesis and transport genes occurred as early as 10–14 dpi in CO-treated plants (MYC + CO vs CTR). A rather different scenario was recorded in CO-treated plants that were not inoculated with AMF (CTR + CO vs CTR, Dataset S1). Under these conditions, SL biosynthesis and

New Phytologist

Table 1 Main arbuscular mycorrhiza (AM) symbiosis-related gene categories impacted at 10 d postinoculation (dpi) by chitooligosaccharides (CO) treatment.

Gene ID	MYC vs CTR	MYC + CO vs CTR	CTR + CO vs CTR	MYC + CO vs MYC	Annotation
Log_2 fold-change value					*Strigolactone signaling*
Medtr3g045440	nr	nr	1.21	nr	Sigma factor sigb regulation rsbq-like protein DLK2
Medtr3g110195	nr	0.35	1.00	nr	Retinal pigment epithelial membrane protein CCD8b
Medtr3g104560	nr	0.47	1.13	nr	Cytochrome P450 family protein MAX1a
Medtr7g045370	nr	nr	0.66	nr	Carotenoid cleavage dioxygenase CCD7
Medtr1g471050	nr	0.75	0.63	nr	Beta-carotene isomerase D27
Medtr3g109610	nr	nr	0.94	nr	Carotenoid cleavage dioxygenase CCD8-1
Medtr3g107870	nr	nr	1.41	nr	Drug resistance transporter-like ABC domain protein PDR1a
Medtr7g063800	nr	nr	1.52	nr	Carotenoid cleavage dioxygenase CCD8-2
					External stimuli response
Medtr5g076900	nr	5.82	nr	nr	Glutathione *S*-transferase amino-terminal domain protein
Medtr5g035640	nr	4.73	nr	nr	Polygalacturonase 1 beta-like protein 3
Medtr7g068600	nr	3.91	nr	nr	myb-like transcription factor family protein MYB1
Medtr1g040500	1.04	3.73	nr	nr	Glycerol-3-phosphate acyltransferase RAM2
Medtr1g109110	0.82	3.02	nr	nr	Palmitoyl-acyl carrier thioesterase FatM
Medtr6g011490	nr	2.56	nr	nr	AP2 domain transcription factor RAM1
Medtr4g104020	0.77	2.26	nr	nr	GRAS family transcription factor RAD1
Medtr5g030910	1.13	1.19	nr	−0.94	Lipid transporter STR
					Cytoskeleton organization
Medtr6g082470	nr	0.93	nr	1.20	ATP-binding microtubule motor family protein
Medtr1g082920	nr	0.79	nr	1.20	Kinesin motor domain protein
Medtr5g094310	nr	0.79	nr	1.15	Kinesin motor domain protein
Medtr7g091290	nr	0.71	nr	1.07	Kinesin motor catalytic domain protein
Medtr1g075680	nr	0.74	nr	1.06	Kinesin motor domain protein
Medtr6g053680	nr	0.75	nr	1.03	ATP-binding microtubule motor family protein
Medtr7g061020	nr	0.80	nr	0.96	ATP-binding microtubule motor family protein
Medtr2g010760	nr	0.73	nr	0.96	Kinesin motor catalytic domain protein
Medtr4g092140	nr	0.68	nr	0.95	Kinesin motor catalytic domain protein
Medtr1g017540	nr	0.62	nr	0.93	Kinesin motor catalytic domain protein
Medtr5g031470	nr	0.68	nr	0.93	Kinesin motor domain Di-glucose-binding protein
Medtr3g107650	0.74	1.65	nr	−0.91	Kinesin-associated protein
					Cell cycle organization
Medtr3g102530	−0.62	0.59	nr	1.21	Carboxy-terminal domain cyclin, Cyclin A
Medtr7g113510	nr	0.94	nr	1.19	Cyclin family protein, putative; mitosis division plane proteinTAN1
Medtr3g110405	nr	0.88	nr	1.16	Serine/Threonine-kinase aurora-like protein, homolog to AtAUR1
Medtr5g088980	nr	0.80	nr	1.15	Carboxy-terminal domain cyclin, Cyclin B
Medtr3g088415	nr	0.85	nr	1.11	Carboxy-terminal domain cyclin, Cyclin A
Medtr5g012010	nr	0.73	nr	1.10	Syntaxin of plants 122 protein, KNOLLE protein
Medtr8g074000	nr	0.84	nr	1.06	Carboxy-terminal domain cyclin, Cyclin B
Medtr7g089080	nr	0.71	nr	1.05	Cyclin B
Medtr5g023790	nr	0.73	nr	1.02	Carboxy-terminal domain cyclin, Cyclin B
Medtr5g011390	nr	0.71	nr	0.86	Cell cycle regulated microtubule-associated protein, AURORA
					Cell wall organization
Medtr8g009560	nr	1.73	1.45	nr	Fatty acid hydroxylase superfamily protein
Medtr7g062250	nr	1.52	nr	1.15	Laccase/diphenol oxidase family protein
Medtr5g075320	nr	1.30	nr	0.93	Expansin A10
Medtr2g097030	nr	1.20	0.88	0.68	Expansin A10
Medtr4g053380	nr	1.12	nr	1.41	Fasciclin-like arabinogalactan protein
Medtr4g081950	nr	1.04	nr	nr	Expansin-A1-like protein
Medtr5g079950	nr	1.03	0.90	0.62	Expansin A10
Medtr2g086070	nr	−1.00	−0.72	nr	Gland-specific fatty acyl-CoA reductase
Medtr4g019225	nr	−1.07	nr	nr	Laccase/diphenol oxidase family protein
Medtr3g098980	nr	−1.10	−0.70	−0.83	Omega-hydroxypalmitate O-feruloyl transferase
Medtr6g086365	−1.16	nr	−2.20	nr	Arabinogalactan protein
Medtr6g086390	nr	nr	−1.59	nr	Arabinogalactan peptide-like protein
Medtr4g059720	nr	nr	nr	0.83	Fasciclin-like arabinogalactan protein
Medtr5g081810	nr	nr	nr	1.18	Laccase/diphenol oxidase family protein

CTR, control; MYC, mycorrhizal; nr, not significantly regulated.

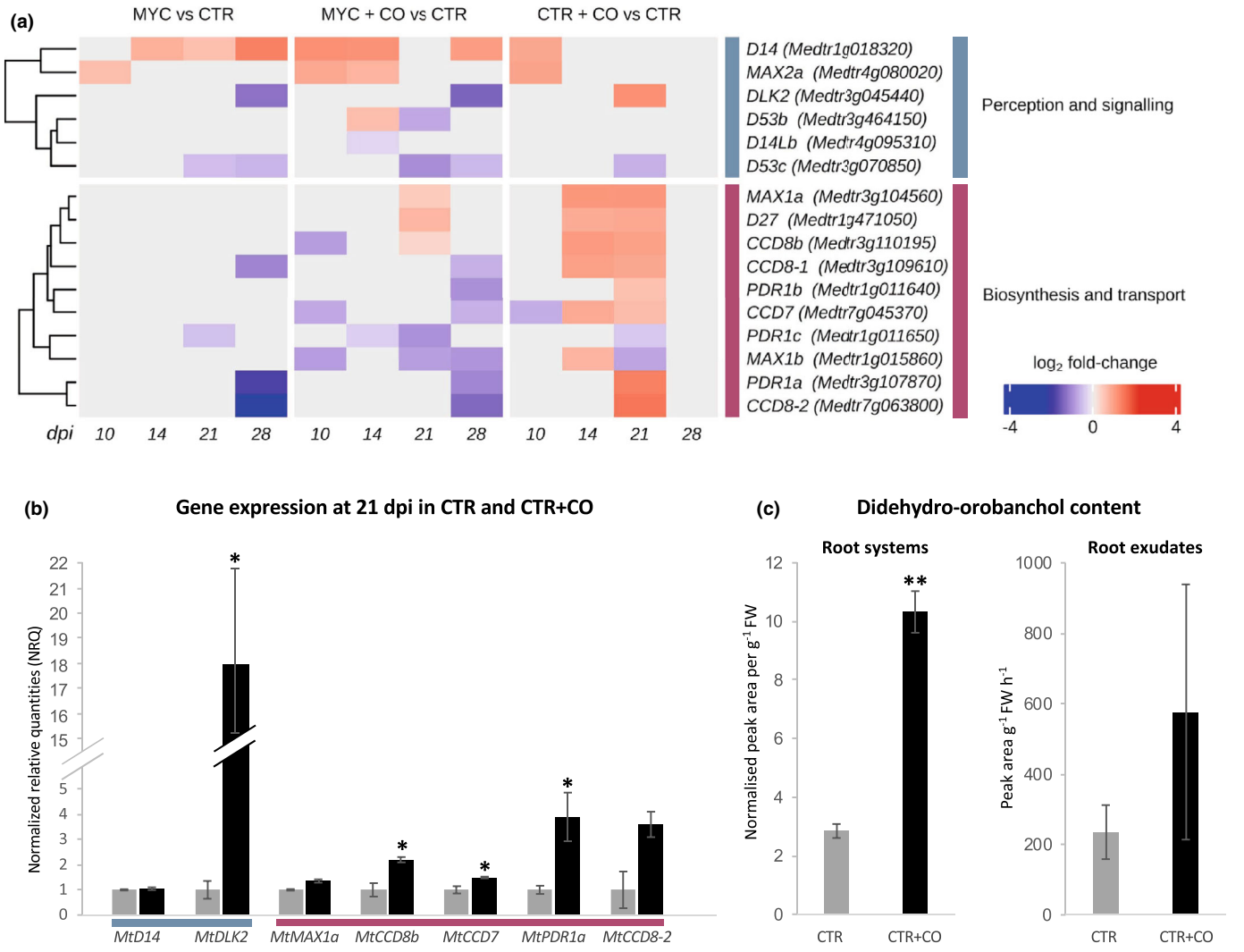

Fig. 2 Chitooligosaccharides (CO) effect on strigolactone (SL)-related gene expression and SL accumulation. (a) Heatmap plot of SL-related genes in each comparison and time points. A progressive decrease in SL biosynthesis (blue) is in line with the progress of arbuscular mycorrhiza (AM) development in mycorrhizal (MYC) vs control (CTR). This downregulation was earlier and more extensive in MYC + CO vs CTR comparison, in line with the acceleration of colonization observed in the presence of CO treatment. Remarkably, a strong upregulation (red) was evident in both SL biosynthesis and transport until 21 d postinoculation (dpi) in the CTR + CO vs CO comparison. Genes are clustered within each category according to Spearman's distance (Müller *et al*., 2019). (b) Independent experiment confirming SL gene expression analysis in CO treated and untreated roots at 21 dpi. Mean values ± SEs of three biological replicates for each treatment are shown. Asterisks indicate statistically significant differences (Student's *t*-test): *, $P < 0.05$. (c) Didehydro-orobanchol (DDO) content in root tissues and exudates of CTR and CTR + CO plants sampled at 21 dpi. A significant increase in DDO root content correlated with CO treatment. A similar trend was observed in the exudates, even if the difference between CTR and CTR + CO plants was statistically not significant. Mean values ± SDs of four biological replications for each treatment are shown. Each biological replication was composed by two plants. Asterisks indicate statistically significant differences (Student's *t*-test: **, $P < 0.01$).

transport-related genes were found to be upregulated between 14 and 21 dpi. Such an upregulation of SL-related genes suggests a CO-dependent boosting of fungus-directed signaling in the absence of an effective interaction with the symbiont.

An independent experiment confirmed a comparable pattern of gene regulation at 21 dpi in CTR + CO compared with CTR plants, with an unchanged expression of *MtD14*, a significant upregulation of *MtDLK2*, *MtCCD8b*, *MtCCD7*, and *MtPDR1a* and a comparable (albeit not significant) trend for *MtMAX1a* and *MtCCD8-2* (Fig. 2b).

To correlate the observed regulation of SL-related gene expression to SL metabolomics, we analyzed SL content in root tissues and exudates from 21-d-old CTR and CTR + CO plants. In our samples, only one SL, didehydro-orobanchol (DDO), was above the detection level. This SL has been identified in roots of several AM host plants (López-Ráez *et al*., 2008; Yoneyama *et al*., 2008; Kohlen *et al*., 2012), and characterized as the major strigolactone in *M. truncatula*, with a role in stimulating hyphal branching in the AM fungus *Gigaspora margarita* (Liu *et al*., 2011; Tokunaga *et al*., 2015). Interestingly, CTR + CO roots contained a significantly higher level of DDO than CTR roots. A comparable trend (albeit statistically not significant) was also observed in root exudates (Fig. 2c).

Second, MYC + CO vs CTR and MYC + CO vs MYC comparisons (Table 1; Datasets S4, S5) highlighted the upregulation

of a consistent group of functional categories related to cell remodeling, such as *Cytoskeleton Organization* and *Cell Wall Organization*. This is in line with the activation of intracellular fungal accommodation by the host tissues (Luginbuehl & Oldroyd, 2017; Pimprikar & Gutjahr, 2018), requiring the reorganization of cytoskeletal elements (Genre *et al.*, 2005), the onset of massive exocytic processes (Genre *et al.*, 2012), cell wall material deposition and remodeling (Balestrini & Bonfante, 2014) to generate the symbiotic interface (Balestrini *et al.*, 2005). Furthermore, a significant upregulation was also observed in *Cell Cycle Organization* for numerous cell cycle regulators (*CYCA*, *CYCB*, *alpha-AURORA kinase activator*) and cell plate-associated proteins (*KNOLLE*), in strong agreement with the described activation of cell division (Russo *et al.*, 2018) and endoreduplication (Carotenuto *et al.*, 2019) as part of the fungal accommodation response.

In the light of this data, and because fungal accommodation responses such as prepenetration apparatus (PPA) development are known to occur in the range of a few hours (Genre *et al.*, 2005), we decided to further investigate earlier responses to CO, by applying local, 6-h-long treatments to *M. truncatula* ROCs (Fig. 3) and analyzing the regulation of *MtKNOLLE* (Richter *et al.*, 2014; Russo *et al.*, 2019) and two additional cell cycle-related markers known to be expressed in early AM development, *MtAPC2*, the *alpha subunit of the Adaptor Protein complex2* (Van Damme *et al.*, 2011; Russo *et al.*, 2018) and *MtCYCL3*, a cyclin-like F-box protein (Russo *et al.*, 2019). Two additional early symbiotic markers were also analyzed: *MtPUB1* (*Plant U-box protein1*), an E3 ubiquitin ligase (Vernié *et al.*, 2016) and *MtCBF3*, a CAAT box-binding transcription factor (Hogekamp *et al.*, 2011).

As shown in Fig. 3, each gene was upregulated upon either 1 g l^{-1}, 1 mg l^{-1}, or 1 µg l^{-1} CO treatment, with 1 mg l^{-1} CO solution resulting to significantly upregulate *MtPUB1*, *MtCBF3*, *MtVapyrin*, *MtKNOLLE*, and *MtAPC2*, whereas *MtCYCL3* was significantly induced only in response to 1 g l^{-1} treatment. By comparing these results with the available data on the Noble *MtGEA V3* database (Benedito *et al.*, 2008; https://lipm-browsers.toulouse.inra.fr/pub/expressionAtlas/app/mtgeav3), we observed a general overlap with the regulation of the same genes during early root-fungus contact (Ortu *et al.*, 2012) and 6 h LCO treatment (Czaja *et al.*, 2012).

In conclusion, our targeted investigation of gene expression confirmed the CO-dependent activation of several early AM markers and revealed that a 6-h CO application is sufficient to activate a set of genes related to prepenetration responses. Together, this gene expression pattern corroborated our RNA-seq data and was fully compatible with the observed acceleration of AM development in CO-treated plants, providing molecular evidence in favor of a CO-dependent advance of prepenetration responses in root cells.

CO treatment stimulated prepenetration responses upon AM inoculation

We then decided to investigate the effect of CO treatment on prepenetration responses in the presence of an AM fungal inoculum. To this aim, we grew *M. truncatula* ROCs expressing GFP-HDEL in the presence of 1 mg l^{-1} CO solution (the most active concentration in our gene expression analyses) or sterile water as a control. GFP-HDEL is a fluorescent marker for the endoplasmic reticulum (ER) that has previously been used to track cytoplasmic aggregations and PPA development during AM colonization (Genre *et al.*, 2005, 2008, 2012). The asynchronous progression of hyphal development and root colonization limits our ability to fully control the timing of fungus–plant contact even using the so-called targeted inoculation method that we here adapted (Chabaud *et al.*, 2002). For this reason, observations were done at 7, 10, or 14 dpi with pregerminated *G. margarita* spores, a time frame that corresponds to hyphopodium formation and initial epidermis colonization. Using hyphopodia as a hallmark to locate plant–fungus contact sites, we focused our observations on the surrounding epidermal cells. As expected,

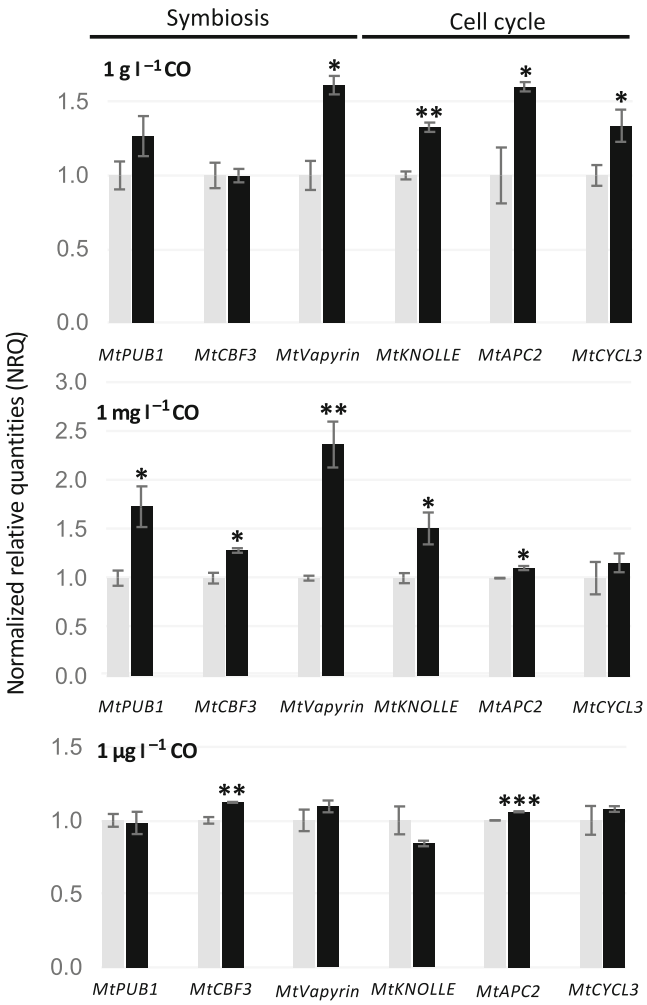

Fig. 3 Local regulation of early arbuscular mycorrhiza (AM) marker genes. Local chitooligosaccharides (CO) treatment stimulated concentration-independent expression of several genes involved in fungal accommodation. The highest number of significantly upregulated genes was recorded upon 1 mg l^{-1} CO application. Grey bars, control, water treated roots; black bars, CO treated roots. Mean values ± SEs of five biological replicates for each treatment are shown. Asterisks indicate statistically significant differences (Student's *t*-test): *, $P < 0.05$; **, $P < 0.01$; ***, $P < 0.001$.

broad ER aggregations were observed at all time points, extending between the hyphopodium contact site and the epidermal cell nucleus, as previously described during PPA formation (Genre *et al.*, 2005). Such aggregations were observed both in the presence or in the absence of the CO treatment. Nevertheless, such PPA-related ER aggregations appeared to be more frequent in CO-treated roots, as confirmed by quantitative analysis (Fig. 4). Indeed, the percent of cells showing ER aggregations in hyphopodium-contacted areas was significantly higher in treated than untreated roots both at 7 and at 10 dpi, while the two data were comparable at 14 dpi. The major impact of CO treatment on earlier time points can be explained with the progressive decrease in residual CO concentration and/or the inhibition of new hyphopodium formation as arbuscules start developing in the inner root tissues. In this scenario, the observed significant stimulation of prepenetration responses in early time points provides a functional validation of our transcriptomic data (Table 1) and the first cellular basis for the observed CO-dependent promotion of AM colonization (Volpe *et al.*, 2020).

Long-term effects of the CO treatment

The 28 dpi time point was associated with a significant increase in plant development for MYC + CO than MYC plants (Fig. S7a). According to our previous studies (Volpe *et al.*, 2020), this is also the time of maximum AM development in our pot cultured *M. truncatula*. This was confirmed by our quantitative analysis, which also highlighted a significant promotion of AM colonization in MYC + CO compared with MYC plants (Fig. S7b). Nevertheless, when comparing MYC + CO to MYC root transcriptome and to MtExpress V3 gene expression data (Carrere *et al.*, 2021), we observed a surprising decline in the expression of several AM markers, including transcription factors (*MtMYB* and *MtRAM2*) and arbuscule-specific phosphate (*MtPT4*) and ammonium (*MtAMT1*) transporters (Fig. 5a; Dataset S4). We suspected that this could indicate the inception of symbiosis senescence, possibly related to space limitations to root development in our pot cultures: in fact, the root system of MYC + CO plants had extended to the whole substrate volume at 28 dpi, which was not the case for MYC plants.

We therefore used confocal microscopy to image and compare arbuscule morphology in MYC and MYC + CO root samples. To obtain a more dynamic view of the colonization process, we extended our analysis to both 21 and 28 dpi. Selected roots were stained with WGA-FITC for detailed imaging of the fungal cell wall and individual arbuscules were classified into four developmental stages based on their morphological features to generate a quantitative comparison (Fig. 5b): Stage I (developing arbuscules with a limited number of large branches); Stage II (intermediate maturity, with several fine branching occupying part of the host cell lumen); Stage III (mature arbuscules, with fine branches in most of the host cell volume); Stage IV (senescent arbuscules displaying clusters of collapsed branches). As shown in the histogram of Fig. 5(b), arbuscule morphology in MYC and MYC + CO plants was comparable at 21 dpi, even if a nonsignificant decrease in Stage II and an increase in Stage IV arbuscules was observed. Interestingly, this trend became more evident – and statistically significant – at 28 dpi, where the arbuscule population in MYC + CO plants also displayed a significant increase in Stage III. At 28 dpi, this resulted in a shift in the distribution of arbuscule classes, with a maximum frequency in Stage II for MYC plants and in Stage III for MYC + CO plants. Altoghether, we interpret this developmental shift as the consequence of the CO-induced advancement in fungal accommodation responses –

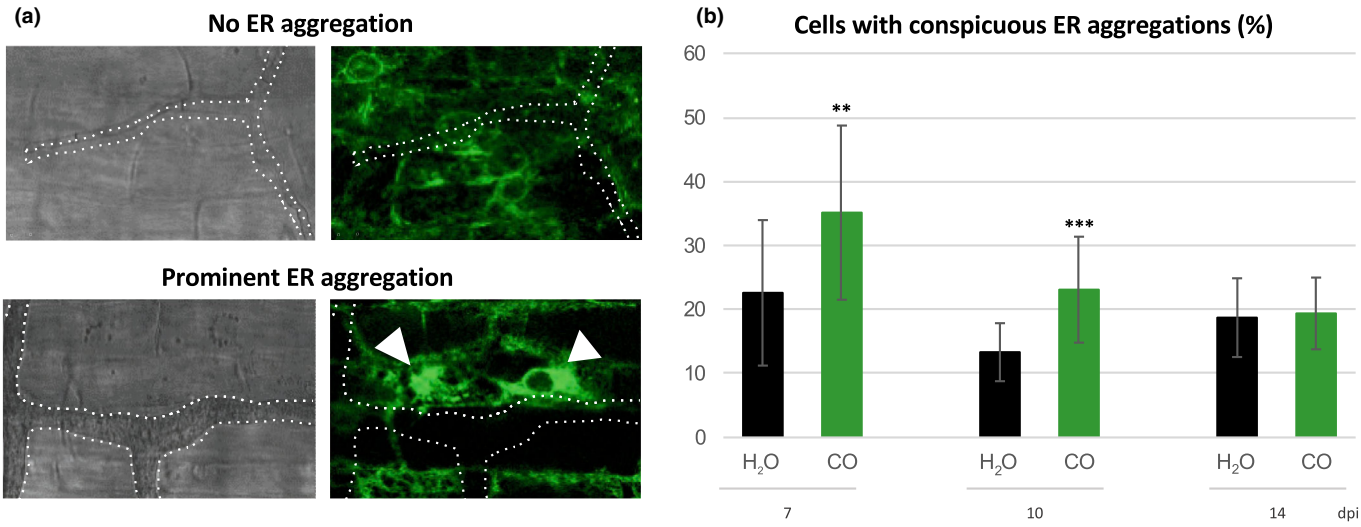

Fig. 4 Prepenetration apparatus (PPA) formation in epidermal cells of *Medicago truncatula*. Root organ cultures expressing GFP-HDEL in the endoplasmic reticulum (ER) were treated with 1 mg l^{-1} chitooligosaccharides (CO) or water (H_2O) as control at the time of inoculation with pregerminated *Gigaspora margarita* spores. Epidermal cells in the vicinity of fungal hyphopodia (dashed white outline) were then imaged at 7, 10, 14 d postinoculation (dpi) and categorized based on the absence or presence of ER aggregations (arrowhead) (a). A statistically significant increase in the percentage of epidermal cells with prominent ER aggregation was recorded in CO-treated roots at 7 and 10 dpi (b). At least 100 independent infection events were visualized for each treatment, error bars indicate SD. Asterisks indicate statistically significant differences (Student's *t*-test): **, $P < 0.01$; ***, $P < 0.001$.

(a)

Gene ID	Log$_2$ fold-change 21 dpi		28 dpi		Annotation	MtExpress V3 value_Log$_2$	
	MYC vs CTR	MYC+CO vs CTR	MYC vs CTR	MYC+CO vs CTR			
Medtr1g028600	6.95	8.29	8.49	6.87	*MtPT4*	Rhizophagus_Arbuscules	9.55
Medtr7g068600	2.16	8.45	8.16	6.90	*MtMYB*	Rhizophagus_Arbuscules	13.2
Medtr1g036410	1.64	6.97	7.44	6.06	*MtAMT1*	Rhizophagus_Arbuscules	7.55
Medtr1g040500	5.30	6.59	7.22	6.47	*MtRAM2*	Rhizophagus_Arbuscules	7.78
Medtr4g093845	5.14	6.14	6.46	5.16	*MtABC*	Rhizophagus_Arbuscules	5.93
Medtr5g011320	5.27	6.75	7.60	6.26	*MtSubtilisin*	No data	-
Medtr5g076900	2.80	8.12	8.11	6.46	*MtGST*	Rhizophagus_Arbuscules	12.7
Medtr5g031090	7.14	7.83	8.09	6.29	*MtLectin*	Rhizophagus_Arbuscules	7.24
Medtr8g006790	3.69	7.63	7.48	6.36	*MtHA1*	Rhizophagus_Arbuscules	8.07

(b)

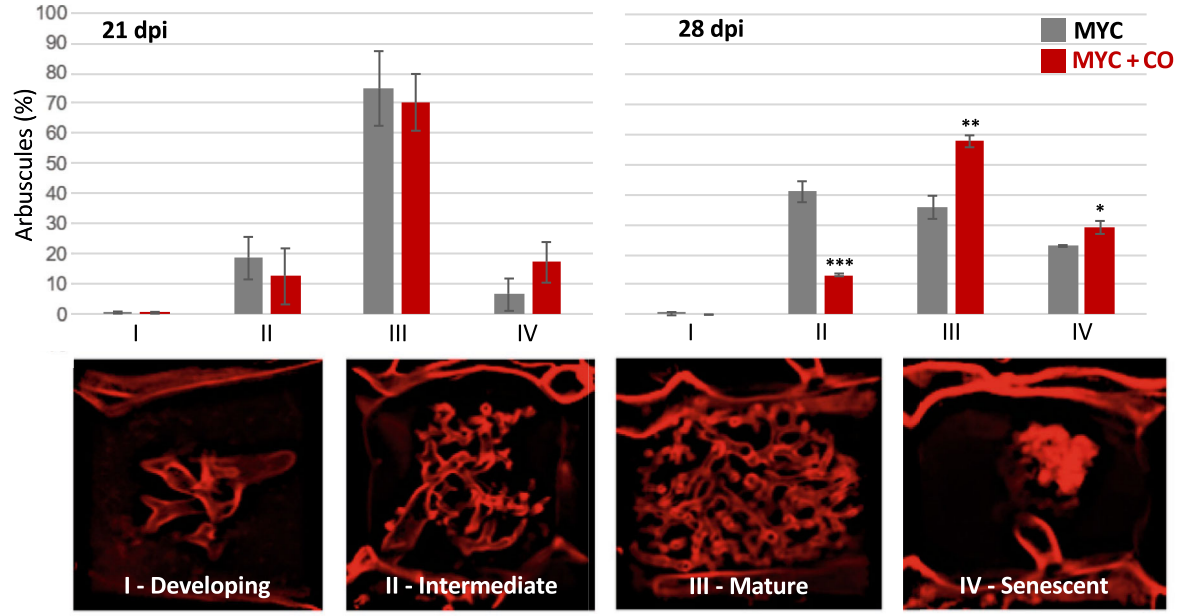

Fig. 5 Quantitative analyses of mycorrhizal phenotypes between mycorrhizal (MYC) and MYC + chitooligosaccharides (CO) plants. (a) Expression of arbuscular mycorrhiza (AM)-induced genes increased at 21 but declined at 28 d postinoculation (dpi) in the comparison MYC + CO vs control (CTR) compared with MYC vs CTR, suggesting the onset of arbuscule senescence at the latest time point. Normalized $\log_2$ expression values from Expression Atlas of Medicago (MtExpress V3; Reference dataset 20220901; https://lipm-browsers.toulouse.inra.fr/pub/expressionAtlas/app/v3/) are reported in the right column. (b) Arbuscules were imaged at 21 and 28 dpi in MYC and MYC + CO plants and classified based on their developmental stage: developing arbuscules with a trunk and very few branches (Stage I), intermediate arbuscules with thick branches (Stage II), fully mature arbuscules with abundant fine branches (Stage III), and senescent arbuscules with clusters of collapsed branches (Stage IV). A comparable distribution between MYC and MYC + CO plants was observed at 21 dpi, even if a nonsignificant reduction and increase were, respectively, observed in Stage II and Stage IV arbuscules. Such trends became statistically significant at 28 dpi, associated with an increase in the abundance of Stage III arbuscules in MYC + CO plants. Data are based on the measurements of 30 infection units for each of four biological replicates. Mean values ± SDs of four biological replications for each treatment are shown. Asterisks indicate statistically significant differences (Student's *t*-test): *, $P < 0.05$; **, $P < 0.01$; ***, $P < 0.001$.

as indicated by our molecular analyses and further demonstrated in epidermal cells by live cell imaging – culminating in a significant advance in arbuscule development and senescence in CO-treated plants.

CO promotion of AM development depends on DMI3

In a previous study, we demonstrated the promotion of AM colonization by CO treatment (Volpe *et al.*, 2020), confirmed also in this study (Fig. S7b). In order to verify whether the observed effect was dependent on CSSP-mediated CO perception, we now applied the same CO treatment to *dmi3-1* mutant plants (Lévy *et al.*, 2004; Mitra *et al.*, 2004) and compared the AM phenotype at 28 dpi between treated and untreated roots. The *M. truncatula Dmi3* gene encodes a nuclear localized Ca^{2+} and calmodulin-dependent kinase that is a central hub of the CSSP (Choi *et al.*, 2018). Its mutation blocks AM colonization at the root epidermis. As described in the literature, the only recognizable

fungal structures associated with *dmi3-1* roots were hyphopodia, while no intraradical fungal development was observed in any of our samples, independent of the CO treatment. Furthermore, our quantitative analysis revealed a comparable abundance of hyphopodia developed in the presence or absence of the CO treatment (Fig. S8a). Such a lack of any evident effect associated with the CO treatment in the *dmi3-1* mutant, strongly suggested that the effects observed in WT plants depend on the CSSP activity.

In an additional set of experiments, we investigated the transcriptional response to COs in *dmi3-1* ROCs, by testing the expression of early AM markers (*MtPUB1*, *MtCBF3*, and *MtVapyrin*) and prepenetration-related genes (*MtKNOLLE*, *MtAPC2*, and *MtCYCL3*; Fig. S8b). The regulation of five out of those six genes (*MtCBF3*, *MtVapyrin*, *MtKNOLLE*, *MtAPC2*, and *MtCYCL3*) was comparable with that reported in the central panel of Fig. 3 for the WT. This upregulation of AM responsive genes in *dmi3* mutants exposed to AM fungal signals has indeed been reported in *M. truncatula* (Kosuta *et al.*, 2003) and rice (Gutjahr *et al.*, 2009), and interpreted as clue to the existence of alternative signaling, acting in parallel to at least one part of the CSSP. A remarkable exception is represented by *MtPUB1*, which was significantly induced in WT samples but downregulated in *dmi3-1* mutants, in line with the canonical CSSP-based model of AM signaling. This pattern of gene regulation, including *Dmi3*-dependence of *MtPUB1*, is comparable with the results of previous studies on early root-fungus contact (Ortu *et al.*, 2012) and 6 h LCO application (Czaja *et al.*, 2012).

Discussion

The main aim of this investigation was to test the hypothesis that CO stimulate symbiotic responses in the host root throughout AM development. In fact, we recently demonstrated that early CO treatment promotes root infection by AM fungi over 28–48 d (Volpe *et al.*, 2020), but a major gap was left in our understanding of the impact of CO treatment on root transcriptome, metabolism, and cellular responses throughout AM colonization.

Indeed, several studies have investigated early plant responses to exogenous treatment with AM fungal raw exudates or purified LCO and CO, revealing the rapid (< 1 h) activation of plant symbiotic signaling processes (Maillet *et al.*, 2011; Genre *et al.*, 2013) and short-term (1–48 h) transcriptional reprogramming (Czaja *et al.*, 2012; Giovannetti *et al.*, 2015; Feng *et al.*, 2019). All of these investigations were anyway analyzing plant responses occurring in the absence of any fungal inoculation.

By analyzing the root transcriptome alongside symbiosis development in a period of over four weeks following initial CO treatment, the present study breaks through this limitation. The consolidation of our gene expression analysis with functional insights generated a first, consistent outlook on CO-dependent plant responses. At any rate, our large transcriptomic dataset, combining four different conditions and four time points, remains available (link in Data availability) to drive further investigations.

Exogenous CO stimulate plant symbiotic responses throughout AM development

Our present results demonstrate that, besides the well-characterized activation of early symbiotic signaling and gene regulation, CO also influenced key symbiotic features of the host tissues from as soon as 6 h after treatment to 28 dpi. Altogether, CO impacted on the expression of root genes related to SL metabolism and transport, altered root SL content; repressed pathogenesis-related genes, and actors of effector-triggered immunity and gene pathways involved in secondary metabolism (isoflavonoid and terpenoid synthesis); increased the expression of lipid and mineral nutrient transporters, globally suggesting the reinforcement of the host response to the AM fungus and the promotion of a symbiosis-oriented metabolic and physiological context. Furthermore, CO also promoted the expression of genes involved in cell-cycle reactivation and fungus accommodation, in association with an observed induction of prepenetration responses, and caused an advance in the root colonization process that extended to 28 dpi.

In short, our experimental results indicate a general and long-lasting stimulation of symbiotic responses in both inoculated and

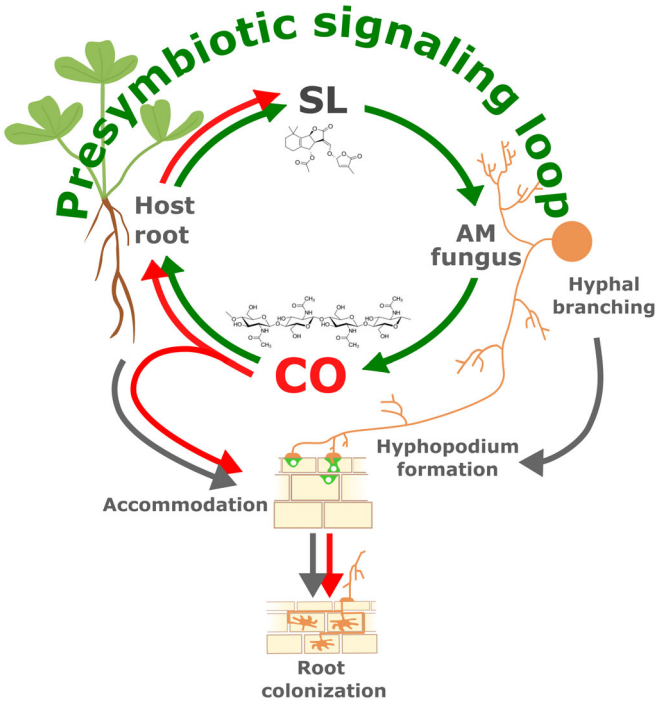

Fig. 6 Schematic representation of exogenous chitooligosaccharides (CO) effects on arbuscular mycorrhiza (AM) symbiosis development. The perception of root-released strigolactones (SL) by AM fungi is known to induce hyphal branching and boost CO release. In turn, CO perception activates root symbiotic responses leading to intracellular fungal accommodation and symbiosis establishment (grey arrows). Our current results (red arrows) indicate that exogenous CO application further stimulates SL biosynthetic gene expression and SL accumulation in the host root, suggesting the presence of a positive feedback mechanism that we propose here as a presymbiotic signaling loop (green arrows). As an additional consequence of CO application, we also observed a stimulation of intracellular fungal accommodation, supporting the observed advance in root colonization and symbiosis development.

uninoculated CO-treated plants, demonstrating that CO have all the predicted features of Myc-factors, intended as fungal-secreted molecules that prepare the host plant to symbiosis establishment (Gutjahr & Parniske, 2013) and actively promote it.

The strange case of an unattainable love

Root exposure to fungal signaling molecules in the absence of the fungus (our CTR + CO condition) represents a markedly artificial situation. In nature, as AM fungal hyphae approach a host root, Myc-factor perception takes place alongside (or shortly before) additional, largely uncharacterized signals (Bonfante & Requena, 2011), including the physical contact between hyphae and root epidermal cells, and the subsequent development of intraradical colonization (Choi *et al.*, 2018). The progression of AM development has an impact on root responses, by transiently triggering defense reactions (García-Garrido & Ocampo, 2002; Jung *et al.*, 2012; Cameron *et al.*, 2013), progressively reducing SL synthesis and secretion (López-Ráez *et al.*, 2011; this paper) and overall outlining the context of a successful symbiotic interaction. By contrast, our CTR + CO plants lack this second set of fungal stimuli, which are crucial modulators of the host response. When interpreting the gene regulation pattern in these root samples, the presence of a certain degree of overreaction should therefore be taken into account. With this caveat, the CTR + CO condition provided the experimental tool to dissect otherwise unseen CO effects. A remarkable example of this artificial amplification of plant responses is the boosting of SL-related gene expression, which extended for a few weeks after CO treatment in CTR + CO plants. We interpret this as a climax in plant presymbiotic signaling, in a condition where physical plant–fungus interaction is not going to occur. While the biological significance of this observation can be limited, with reference to a natural context, it convincingly indicates that CO effects extend over several weeks and impact on SL content, a root feature that is directly linked to AM symbiosis establishment.

A symbiotic signaling loop?

Plants exude diverse mixtures of SL, depending on plant species, growth conditions, and developmental stages (Wang & Bouwmeester, 2018). With reference to AM signaling, DDO has been characterized as the most active molecule in *M. truncatula* (López-Ráez *et al.*, 2008; Yoneyama *et al.*, 2008; Kohlen *et al.*, 2012). In this frame, our novel observation of SL metabolism-related gene upregulation upon CO treatment is further reinforced by DDO accumulation in the root, suggesting a redirection of SL metabolism toward AM fungus-directed signals in CO-treated roots.

Furthermore, previous investigations have recorded an increase in CO release by SL-treated AM fungi (Genre *et al.*, 2013). Altogether, this suggests the existence of a positive feedback mechanism that reinforces reciprocal plant–fungus signaling in support of symbiosis establishment.

To summarize our conclusions, we propose a model – schematized in Fig. 6 – where the exogenous application of CO does not only boost signal exchange in this symbiotic signaling loop, but also stimulates intracellular accommodation responses in the host root, facilitating fungal colonization and eventually accelerating symbiosis development.

Acknowledgements

We are grateful to David Barker and Paola Bonfante for constructive discussion and their critical revision of the manuscript draft. We also thank David Barker to kindly providing *Medicago dmi3-1* mutant seeds. This research was funded by Fondazione Cassa di Risparmio di Cuneo (Bando Ricerca Scientifica 2015 – Project AM for Quality 2015/17271). We are grateful to Erik Limpens for hosting LC in his laboratory in Wageningen for an Erasmus+ traineeship.

Competing interests

None declared.

Author contributions

VV and TM performed experiments and data analysis. MC performed data analysis and contributed figure editing and manuscript writing. AC, SC, LC and WK performed experiments. VV and AG conceived experiments and wrote the manuscript.

ORCID

Serena Capitanio https://orcid.org/0000-0002-1609-0499
Matteo Chialva https://orcid.org/0000-0002-6996-6642
Lorenzo Costamagna https://orcid.org/0000-0003-1129-6495
Andrea Crosino https://orcid.org/0000-0001-6219-1920
Andrea Genre https://orcid.org/0000-0001-5029-6194
Wouter Kohlen https://orcid.org/0000-0001-9057-2392
Teresa Mazzarella https://orcid.org/0000-0003-3435-3771
Veronica Volpe https://orcid.org/0000-0002-3559-7615

Data availability

Raw RNA-seq data are openly available in the NCBI Sequence Read Archive (SRA) under BioProject accession no. PRJNA813377.

References

Akiyama K, Matsuzaki K, Hayashi H. 2005. Plant sesquiterpenes induce hyphal branching in arbuscular mycorrhizal fungi. *Nature* **43**: 824–827.
Anders S, Pyl PT, Huber W. 2015. HTSeq – a Python framework to work with high-throughput sequencing data. *Bioinformatics* **31**: 166–169.
Balestrini R, Bonfante P. 2014. Cell wall remodeling in mycorrhizal symbiosis: a way towards biotrophism. *Frontiers in Plant Science* **5**: 237.
Balestrini R, Cosgrove DJ, Bonfante P. 2005. Differential location of α-expansin proteins during the accommodation of root cells to an arbuscular mycorrhizal fungus. *Planta* **220**: 889–899.
Bécard G, Fortin JA. 1988. Early events of vesicular–arbuscular mycorrhiza formation on Ri T-DNA transformed roots. *New Phytologist* **108**: 211–218.

Benedito VA, Li H, Dai X, Wandrey M, He J, Kaundal R, Torres-Jerez I, Gomez SK, Harrison MJ, Tang Y *et al.* 2010. Genomic inventory and transcriptional analysis of *Medicago truncatula* transporters. *Plant Physiology* **152**: 1716–1730.

Benedito VA, Torres-Jerez I, Murray JD, Andriankaja A, Allen S, Kakar K, Wandrey M, Verdier J, Zuber H, Ott T *et al.* 2008. A gene expression atlas of the model legume *Medicago truncatula*. *The Plant Journal* **55**: 504–513.

Benjamini Y, Hochberg Y. 1995. Controlling the false discovery rate: a practical and powerful approach to multiple testing. *Journal of the Royal Statistical Society: Series B (Statistical Methodology)* **57**: 289–300.

Besserer A, Puech-Pagès V, Kiefer P, Gomez-Roldan V, Jauneau A, Roy S, Portais JC, Roux C, Bécard G, Séjalon-Delmas N. 2006. Strigolactones stimulate arbuscular mycorrhizal fungi by activating mitochondria. *PLoS Biology* **4**: e226.

Boisson-Dernier A, Chabaud M, Garcia F, Bécard G, Rosenberg C, Barker DG. 2001. *Agrobacterium rhizogenes*-transformed roots of *Medicago truncatula* for the study of nitrogen-fixing and endomycorrhizal symbiotic associations. *Molecular Plant–Microbe Interactions* **14**: 695–700.

Bonfante P, Requena N. 2011. Dating in the dark: how roots respond to fungal signals to establish arbuscular mycorrhizal symbiosis. *Current Opinion in Plant Biology* **14**: 451–457.

Cameron DD, Neal AL, van Wees SC, Ton J. 2013. Mycorrhiza-induced resistance: more than the sum of its parts. *Trends in Plant Science* **18**: 539–545.

Camps C, Jardinaud MF, Rengel D, Carrère S, Hervé C, Debellé F, Gamas P, Bensmihen S, Gough C. 2015. Combined genetic and transcriptomic analysis reveals three major signalling pathways activated by Myc-LCOs in *Medicago truncatula*. *New Phytologist* **208**: 224–240.

Carotenuto G, Volpe V, Russo G, Politi M, Sciascia I, de Almeida-Engler J, Genre A. 2019. Local endoreduplication as a feature of intracellular fungal accommodation in arbuscular mycorrhizas. *New Phytologist* **223**: 430–446.

Carrere S, Verdier J, Gamas P. 2021. MtExpress, a comprehensive and curated RNAseq-based gene expression atlas for the model legume *Medicago truncatula*. *Plant and Cell Physiology* **62**: 1494–1500.

Chabaud M, Genre A, Sieberer BJ, Faccio A, Fournier J, Novero M, Barker DG, Bonfante P. 2011. Arbuscular mycorrhizal hyphopodia and germinated spore exudates trigger Ca^{2+} spiking in the legume and nonlegume root epidermis. *New Phytologist* **189**: 347–355.

Chabaud M, Venard C, Defaux-Petras A, Bécard G, Barker DG. 2002. Targeted inoculation of *Medicago truncatula in vitro* root cultures reveals *MtENOD11* expression during early stages of infection by arbuscular mycorrhizal fungi. *New Phytologist* **156**: 265–273.

Choi J, Summers W, Paszkowski U. 2018. Mechanisms underlying establishment of arbuscular mycorrhizal symbioses. *Annual Review of Phytopathology* **56**: 135–160.

Crosino A, Moscato E, Blangetti M, Carotenuto G, Spina F, Bordignon S, Puech-Pagès V, Anfossi L, Volpe V, Prandi C *et al.* 2021. Extraction of short chain chitooligosaccharides from fungal biomass and their use as promoters of arbuscular mycorrhizal symbiosis. *Scientific Reports* **11**: 3798.

Czaja LF, Hogekamp C, Lamm P, Maillet F, Martinez EA, Samain E, Dénarié J, Küster H, Hohnjec N. 2012. Transcriptional responses toward diffusible signals from symbiotic microbes reveal *MtNFP*- and *MtDMI3*-dependent reprogramming of host gene expression by arbuscular mycorrhizal fungal lipochitooligosaccharides. *Plant Physiology* **159**: 1671–1685.

Del Fabbro C, Scalabrin S, Morgante M, Giorgi FM. 2013. An extensive evaluation of read trimming effects on Illumina NGS data analysis. *PLoS ONE* **8**: e85024.

Dobin A, Davis CA, Schlesinger F, Drenkow J, Zaleski C, Jha S, Batut P, Chaisson M, Gingeras TR. 2013. STAR: ultrafast universal RNA-seq aligner. *Bioinformatics* **29**: 15–21.

Feng F, Sun J, Radhakrishnan GV, Lee T, Bozsóki Z, Fort S, Gavrin A, Gysel K, Thygesen MB, Andersen KR *et al.* 2019. A combination of chitooligosaccharide and lipochitooligosaccharide recognition promotes arbuscular mycorrhizal associations in *Medicago truncatula*. *Nature Communications* **10**: 5047.

García-Garrido JM, Ocampo JA. 2002. Regulation of the plant defence response in arbuscular mycorrhizal symbiosis. *Journal of Experimental Botany* **53**: 1377–1386.

Gaude N, Bortfeld S, Duensing N, Lohse M, Krajinski F. 2012. Arbuscule-containing and non-colonized cortical cells of mycorrhizal roots undergo a massive and specific reprogramming during arbuscular mycorrhizal development. *The Plant Journal* **69**: 510–528.

Genre A, Chabaud M, Balzergue C, Puech-Pagès V, Novero M, Rey T, Fournier J, Rochange S, Bécard G, Bonfante P *et al.* 2013. Short-chain chitin oligomers from arbuscular mycorrhizal fungi trigger nuclear Ca^{2+} spiking in *Medicago truncatula* roots and their production is enhanced by strigolactone. *New Phytologist* **19**: 190–202.

Genre A, Chabaud M, Faccio A, Barker DG, Bonfante P. 2008. Prepenetration apparatus assembly precedes and predicts the colonization patterns of arbuscular mycorrhizal fungi within the root cortex of both *Medicago truncatula* and *Daucus carota*. *Plant Cell* **20**: 1407–1420.

Genre A, Chabaud M, Timmers T, Bonfante P, Barker DG. 2005. Arbuscular mycorrhizal fungi elicit a novel intracellular apparatus in *Medicago truncatula* root epidermal cells before infection. *Plant Cell* **17**: 3489–3499.

Genre A, Ivanov S, Fendrych M, Faccio A, Zársky V, Bisseling T, Bonfante P. 2012. Multiple exocytotic markers accumulate at the sites of perifungal membrane biogenesis in arbuscular mycorrhizas. *Plant and Cell Physiology* **53**: 244–255.

Giovannetti M, Mari A, Novero M, Bonfante P. 2015. Early *Lotus japonicus* root transcriptomic responses to symbiotic and pathogenic fungal exudates. *Frontiers in Plant Science* **6**: 480.

Gomez-Roldan V, Fermas S, Brewer PB, Puech-Pagès V, Dun EA, Pillot JP, Letisse F, Matusova R, Danoun S, Portais JC *et al.* 2008. Strigolactone inhibition of shoot branching. *Nature* **455**: 189–194.

Gutjahr C, Novero M, Guether M, Montanari O, Udvardi M, Bonfante P. 2009. Presymbiotic factors released by the arbuscular mycorrhizal fungus *Gigaspora margarita* induce starch accumulation in *Lotus japonicus* roots. *New Phytologist* **183**: 53–61.

Gutjahr C, Parniske M. 2013. Cell and developmental biology of arbuscular mycorrhiza symbiosis. *Annual Review of Cellular and Developmental Biology* **29**: 593–617.

Handa Y, Nishide H, Takeda N, Suzuki Y, Kawaguchi M, Saito K. 2015. RNA-seq transcriptional profiling of an arbuscular mycorrhiza provides insights into regulated and coordinated gene expression in *Lotus japonicus* and *Rhizophagus irregularis*. *Plant and Cell Physiology* **56**: 1490–1511.

Haseloff J, Siemering KR, Prasher DC, Hodge S. 1997. Removal of a cryptic intron and subcellular localization of green fluorescent protein are required to mark transgenic Arabidopsis plants brightly. *Proceedings of the National Academy of Sciences, USA* **94**: 2122–2127.

Hewitt EJ. 1966. Sand and water culture methods used in the study of plant nutrition. *Experimental Agriculture* **3**: 104.

Hogekamp C, Arndt D, Pereira PA, Becker JD, Hohnjec N, Küster H. 2011. Laser microdissection unravels cell-type-specific transcription in arbuscular mycorrhizal roots, including CAAT-box transcription factor gene expression correlating with fungal contact and spread. *Plant Physiology* **157**: 2023–2043.

Hogekamp C, Küster H. 2013. A roadmap of cell-type specific gene expression during sequential stages of the arbuscular mycorrhiza symbiosis. *BMC Genomics* **14**: 306.

Hohnjec N, Vieweg MF, Pühler A, Becker A, Küster H. 2005. Overlaps in the transcriptional profiles of *Medicago truncatula* roots inoculated with two different *Glomus* fungi provide insights into the genetic program activated during arbuscular mycorrhiza. *Plant Physiology* **137**: 1283–1301.

Jung SC, Martinez-Medina A, Lopez-Raez JA, Pozo MJ. 2012. Mycorrhiza-induced resistance and priming of plant defenses. *Journal of Chemical Ecology* **38**: 651–664.

Keymer A, Pimprikar P, Wewer V, Huber C, Brands M, Bucerius SL, Delaux PM, Klingl V, Röpenack-Lahaye EV, Wang TL *et al.* 2017. Lipid transfer from plants to arbuscular mycorrhiza fungi. *eLife* **6**: e29107.

Kohlen W, Charnikhova T, Lammers M, Pollina T, Tóth P, Haider I, Pozo MJ, de Maagd RA, Ruyter-Spira C, Bouwmeester HJ *et al.* 2012. The tomato CAROTENOID CLEAVAGE DIOXYGENASE8 (SlCCD8) regulates rhizosphere signaling, plant architecture and affects reproductive development through strigolactone biosynthesis. *New Phytologist* **196**: 535–547.

Kosuta S, Chabaud M, Lougnon G, Gough C, Dénarié J, Barker DG, Bécard G. 2003. A diffusible factor from arbuscular mycorrhizal fungi induces symbiosis-

specific MtENOD11 expression in roots of *Medicago truncatula*. *Plant Physiology* **131**: 952–962.

Küster H, Hohnjec N, Krajinski F, El Yahyaoui F, Manthey K, Gouzy J, Dondrup M, Meyer F, Kalinowski J, Brechenmacher L *et al.* 2004. Construction and validation of cDNA-based Mt6k-RIT macro- and microarrays to explore root endosymbioses in the model legume *Medicago truncatula*. *Journal of Biotechnology* **108**: 95–113.

Lévy J, Bres C, Geurts R, Chalhoub B, Kulikova O, Duc G, Journet EP, Ané JM, Lauber E, Bisseling T *et al.* 2004. A putative Ca^{2+} and calmodulin-dependent protein kinase required for bacterial and fungal symbioses. *Science* **303**: 1361–1364.

Liu J, Blaylock LA, Endre G, Cho J, Town CD, VandenBosch KA, Harrison MJ. 2003. Transcript profiling coupled with spatial expression analyses reveals genes involved in distinct developmental stages of an arbuscular mycorrhizal symbiosis. *Plant Cell* **15**: 2106–2123.

Liu W, Kohlen W, Lillo A, Op den Camp R, Ivanov S, Hartog M, Limpens E, Jamil M, Smaczniak C, Kaufmann K. 2011. Strigolactone biosynthesis in *Medicago truncatula* and rice requires the symbiotic GRAS-type transcription factors NSP1 and NSP2. *Plant Cell* **23**: 3853–3865.

López-Ráez JA, Charnikhova T, Fernández I, Bouwmeester H, Pozo MJ. 2011. Arbuscular mycorrhizal symbiosis decreases strigolactone production in tomato. *Journal of Plant Physiology* **168**: 294–297.

López-Ráez JA, Charnikhova T, Mulder P, Kohlen W, Bino R, Levin I, Bouwmeester H. 2008. Susceptibility of the tomato mutant *high pigment-2^{dg}* (*hp-2^{dg}*) to *Orobanche* spp. infection. *Journal of Agricultural and Food Chemistry* **56**: 6326–6332.

Love MI, Huber W, Anders S. 2014. Moderated estimation of fold change and dispersion for RNA-seq data with DESeq2. *Genome Biology* **15**: 550.

Luginbuehl LH, Menard GN, Kurup S, Van Erp H, Radhakrishnan GV, Breakspear A, Oldroyd GED, Eastmond PJ. 2017. Fatty acids in arbuscular mycorrhizal fungi are synthesized by the host plant. *Science* **356**: 1175–1178.

Luginbuehl LH, Oldroyd G. 2017. Understanding the arbuscule at the heart of endomycorrhizal symbioses in plants. *Current Biology* **27**: R952–R963.

Luo W, Brouwer C. 2013. Pathview: an R/bioconductor package for pathway-based data integration and visualization. *Bioinformatics* **29**: 1830–1831.

MacLean AM, Bravo A, Harrison MJ. 2017. Plant signaling and metabolic pathways enabling arbuscular mycorrhizal symbiosis. *Plant Cell* **29**: 2319–2335.

Maillet F, Poinsot V, André O, Puech-Pagès V, Haouy A, Gueunier M, Cromer L, Giraudet D, Formey D, Niebel A *et al.* 2011. Fungal lipochitooligosaccharide symbiotic signals in arbuscular mycorrhiza. *Nature* **469**: 58–63.

Martin M. 2011. Cutadapt removes adapter sequences from high-throughput sequencing reads. *EMBnet Journal* **17**: 10–12.

Mitra RM, Gleason CA, Edwards A, Hadfield J, Downie JA, Oldroyd GE, Long SR. 2004. A Ca^{2+}/calmodulin-dependent protein kinase required for symbiotic nodule development: gene identification by transcript-based cloning. *Proceedings of the National Academy of Sciences, USA* **30**: 4701–4705.

Müller LM, Flokova K, Schnabel E, Sun X, Fei Z, Frugoli J, Bouwmeester HJ, Harrison MJ. 2019. A CLE-SUNN module regulates strigolactone content and fungal colonization in arbuscular mycorrhiza. *Nature Plants* **5**: 933–939.

Nasir F, Bahadur A, Lin X, Gao Y, Tian C. 2021. Novel insights into host receptors and receptor-mediated signaling that regulate arbuscular mycorrhizal symbiosis. *Journal of Experimental Botany* **72**: 1546–1557.

Oksanen J, Blanchet FG, Friendly M, Kindt R, Legendre P, McGlinn D, Minchin PR, O'Hara RB, Simpson GL, Solymos P *et al.* 2019. *vegan: community ecology package*. R package v.2.5-5. [WWW document] URL https://CRAN.R-project.org/package=vegan [accessed 27 April 2022].

Ortu G, Balestrini R, Pereira PA, Becker JD, Küster H, Bonfante P. 2012. Plant genes related to gibberellin biosynthesis and signaling are differentially regulated during the early stages of AM fungal interactions. *Molecular Plant* **5**: 951–954.

Pimprikar P, Gutjahr C. 2018. Transcriptional regulation of arbuscular mycorrhiza development. *Plant and Cell Physiology* **59**: 673–690.

R Core Team. 2020. *R: a language and environment for statistical computing*. Vienna, Austria: R Foundation for Statistical Computing. [WWW document] URL https://www.R-project.org/ [accessed 31 May 2021].

Richter S, Kientz M, Brumm S, Nielsen ME, Park M, Gavidia R, Krause C, Voss U, Beckmann H, Mayer U *et al.* 2014. Delivery of endocytosed proteins to the cell-division plane requires change of pathway from recycling to secretion. *eLife* **3**: e02131.

Russo G, Carotenuto G, Fiorilli V, Volpe V, Chiapello M, Van Damme D, Genre A. 2018. Ectopic activation of cortical cell division during the accommodation of arbuscular mycorrhizal fungi. *New Phytologist* **221**: 1036–1048.

Russo G, Carotenuto G, Fiorilli V, Volpe V, Faccio A, Bonfante P, Chabaud M, Chiapello M, Van Damme D, Genre A. 2019. TPLATE recruitment reveals endocytic dynamics at sites of symbiotic interface assembly in arbuscular mycorrhizal interactions. *Frontiers in Plant Science* **10**: 1628.

Salzer P, Bonanomi A, Beyer K, Vögeli-Lange R, Aeschbacher RA, Lange JAW, Kim D, Cook DR, Boller T. 2000. Differential expression of eight chitinase genes in *Medicago truncatula* roots during mycorrhiza formation, nodulation, and pathogen infection. *Molecular Plant–Microbe Interactions* **13**: 763–777.

Sanchez L, Weidmann S, Brechenmacher L, Batoux M, van Tuinen D, Lemanceau P, Gianinazzi S, Gianinazzi-Pearson V. 2004. Common gene expression in *Medicago truncatula* roots in response to *Pseudomonas fluorescens* colonization, mycorrhiza development and nodulation. *New Phytologist* **161**: 855–863.

Schwacke R, Ponce-Soto GY, Krause K, Bolger AM, Arsova B, Hallab A, Gruden K, Stitt M, Bolger ME, Usadel B. 2019. MapMan4: a refined protein classification and annotation framework applicable to multi-omics data analysis. *Molecular Plant* **12**: 879–892.

Sieberer BJ, Chabaud M, Timmers AC, Monin A, Fournier J, Barker DG. 2009. A nuclear-targeted cameleon demonstrates intranuclear Ca^{2+} spiking in *Medicago truncatula* root hairs in response to rhizobial nodulation factors. *Plant Physiology* **151**: 1197–1206.

Smith SE, Read DJ. 2008. *Mycorrhizal symbiosis*. San Diego, CA, USA: Academic Press.

Spatafora JW, Chang Y, Benny GL, Lazarus K, Smith ME, Berbee ML, Bonito G, Corradi N, Grigoriev I, Gryganskyi A *et al.* 2016. A phylum-level phylogenetic classification of zygomycete fungi based on genome-scale data. *Mycologia* **108**: 1028–1046.

Sun J, Miller JB, Granqvist E, Wiley-Kalil A, Gobbato E, Maillet F, Cottaz S, Samain E, Venkateshwaran M, Fort S *et al.* 2015. Activation of symbiosis signaling by arbuscular mycorrhizal fungi in legumes and rice. *Plant Cell* **27**: 823–838.

Tang H, Krishnakumar V, Bidwell S, Rosen B, Chan A, Zhou S, Gentzbittel L, Childs KL, Yandell M, Gundlach H *et al.* 2014. An improved genome release (v.Mt4.0) for the model legume *Medicago truncatula*. *BMC Genomics* **15**: 312.

Tokunaga T, Hayashi H, Akiyama K. 2015. Medicaol, a strigolactone identified as a putative didehydro-orobanchol isomer, from *Medicago truncatula*. *Phytochemistry* **111**: 91–97.

Trouvelot A, Kough JL, Gianinazzi-Pearson V. 1986. Mesure du taux de mycorhization VA d'un système radiculaire. Recherche de methods d'estimation ayant une signification fonctionnelle. In: Gianinazzi-Pearson V, Gianinazzi S, eds. *Physiological and genetical aspects of mycorrhizae*. Paris, France: INRA, 217–221.

Umehara M, Hanada A, Yoshida S, Akiyama K, Arite T, Takeda-Kamiya N, Magome H, Kamiya Y, Shirasu K, Yoneyama K *et al.* 2008. Inhibition of shoot branching by new terpenoid plant hormones. *Nature* **455**: 195–200.

Usadel B, Nagel A, Thimm O, Redestig H, Blaesing OE, Palacios-Rojas N, Selbig J, Hannemann J, Piques MC, Steinhauser D *et al.* 2005. Extension of the visualization tool MapMan to allow statistical analysis of arrays, display of corresponding genes, and comparison with known responses. *Plant Physiology* **138**: 1195–1204.

Van Damme D, Gadeyne A, Vanstraelen M, Inze D, Van Montagu MC, De Jaeger G, Russinova E, Geelen D. 2011. Adaptin-like protein TPLATE and clathrin recruitment during plant somatic cytokinesis occurs via two distinct pathways. *Proceedings of the National Academy of Sciences, USA* **108**: 615–620.

Vernié T, Camut S, Camps C, Rembliere C, de Carvalho-Niebel F, Mbengue M, Timmers T, Gasciolli V, Thompson R, le Signor C *et al.* 2016. PUB1 interacts with the receptor kinase DMI2 and negatively regulates rhizobial and arbuscular mycorrhizal symbioses through its ubiquitination activity in *Medicago truncatula*. *Plant Physiology* **170**: 2312–2324.

Volpe V, Carotenuto G, Berzero C, Cagnina L, Puech-Pagès V, Genre A. 2020. Short chain chitooligosaccharides promote arbuscular mycorrhizal colonization in *Medicago truncatula*. *Carbohydrate Polymers* **229**: 115505.

Wang Y, Bouwmeester HJ. 2018. Structural diversity in the strigolactones. *Journal of Experimental Botany* **69**: 2219–2230.

Waters MT, Gutjahr C, Bennett T, Nelson DC. 2017. Strigolactone signaling and evolution. *Annual Review of Plant Biology* **68**: 291–322.

Wewer V, Brands M, Dörmann P. 2014. Fatty acid synthesis and lipid metabolism in the obligate biotrophic fungus *Rhizophagus irregularis* during mycorrhization of *Lotus japonicus*. *The Plant Journal* **79**: 398–412.

Wickham H. 2016. *GGPLOT2: elegant graphics for data analysis, 2nd edn.* Cham, Switzerland: Springer International.

Yoneyama K, Xie X, Sekimoto H, Takeuchi Y, Ogasawara S, Akiyama K, Hayashi H, Yoneyama K. 2008. Strigolactones, host recognition signals for root parasitic plants and arbuscular mycorrhizal fungi, from Fabaceae plants. *New Phytologist* **179**: 484–494.

Young MD, Wakefield MJ, Smyth GK, Oshlack A. 2010. Gene ontology analysis for RNA-seq: accounting for selection bias. *Genome Biology* **11**: R14.

Young ND, Debellé F, Oldroyd GE, Geurts R, Cannon SB, Udvardi MK, Benedito VA, Mayer KF, Gouzy J, Schoof H *et al.* 2011. The Medicago genome provides insight into the evolution of rhizobial symbioses. *Nature* **480**: 520–524.

Zipfel C, Oldroyd GE. 2017. Plant signaling in symbiosis and immunity. *Nature* **543**: 328–336.

Supporting Information

Additional Supporting Information may be found online in the Supporting Information section at the end of the article.

Dataset S1 RNA-seq-based expression data for all genes expressed in CCO vs C during time-course experiment.

Dataset S2 RNA-seq-based expression data for all genes expressed in M vs C during time-course experiment.

Dataset S3 RNA-seq-based expression data for all genes expressed in MCO vs C during time-course experiment.

Dataset S4 RNA-seq-based expression data for all genes expressed in MCO vs M during time-course experiment.

Dataset S5 Gene Ontology functional enrichments ($P_{adj} < 0.1$) of DEGs list in CTR+CO vs CTR.

Dataset S6 Gene Ontology functional enrichments ($P_{adj} < 0.1$) of DEGs list in MYC vs CTR.

Dataset S7 Gene Ontology functional enrichments ($P_{adj} < 0.1$) of DEGs list in MYC + CO vs CTR.

Dataset S8 Gene Ontology functional enrichments ($P_{adj} < 0.1$) of DEGs list in MYC+CO vs MYC.

Fig. S1 RNA-seq and qRT-PCR data correlation.

Fig. S2 Gene Ontology enrichment analysis in the comparison MYC vs CTR at 10 and 28 dpi.

Fig. S3 Gene Ontology enrichment analysis in the comparison CTR + CO vs CTR at 10 dpi.

Fig. S4 Gene Ontology enrichment analysis in the comparison MYC + CO vs CTR at 10 and 28 dpi.

Fig. S5 Gene Ontology enrichment analysis in the comparison MYC + CO vs MYC at 10 and 28 dpi.

Fig. S6 Gene regulation pattern in CTR + CO and MYC plants compared with CTR.

Fig. S7 Morphological analysis in mychorrized plants.

Fig. S8 CO responses in *dmi3-1* mutants.

Table S1 Summary statistics for the Illumina sequencing and mapping against *M. truncatula* genome assembly, v.4.1.

Table S2 List of overrepresented MapMan functional categories.

Table S3 List of primers used for RNA-seq validation experiments.

Table S4 List of primers used for qRT-PCR experiments.

Please note: Wiley is not responsible for the content or functionality of any Supporting Information supplied by the authors. Any queries (other than missing material) should be directed to the *New Phytologist* Central Office.